Cellulose (2018) 25:3797–3814
https://doi.org/10.1007/s10570-018-1835-y

ORIGINAL PAPER

Insights into degradation pathways of oxidized anhydroglucose units in cellulose by β-alkoxy-elimination: a combined theoretical and experimental approach

Takashi Hosoya · Markus Bacher · Antje Potthast · Thomas Elder · Thomas Rosenau

Received: 12 March 2018 / Accepted: 5 May 2018 / Published online: 17 May 2018

Abstract Depolymerization of cellulose starting from an oxidized anhydroglucose unit through β-alkoxy-elimination, triggered by alkaline media, is one of the key reactions responsible for cellulose aging. This study investigates the detailed mechanisms for the chain cleavage by a combination of experimental and quantum chemical methods. Three model compounds for oxidized anhydroglucose units in cellulose were employed: C2-keto, C3-keto-, and C6-aldehyde 4-*O*-methyl methyl β-D-glucosides, representing anhydroglucose units of cellulose that have been oxidized at C2, C3, and C6, respectively. The alkali-induced β-alkoxy elimination from the model compounds started from the corresponding enolates and followed first order kinetics. While methanol is being released in the case of the model compounds, the analogous process effects chain cleavage in the case of the polymer cellulose. The kinetic rate constants for the C6-aldehyde compound **2**, the 2-keto compound **3** and the 3-keto counterpart **4** had a ratio of 1:5:22, indicating the 3-keto compound to be the least stable one. Elimination from an oxidized 6-position (6-aldehyde) was thus more than 20 times slower than that from an oxidized C-3 (3-keto). A 6-carboxyl group is completely innocent with regard to β-elimination. MP4(SDQ)//DFT(M06-2X) calculations indicated that the degradation pathway starting from the 3-keto enolate had the smallest activation barrier because of stabilization of the transition state by charge transfer from O-5 to C-1. The 3-keto enolate path was consequently more favorable than the alternative ones involving the 2-keto and the 6-keto enolates, which do not exhibit this transition state stabilization. Experimental and computational data thus agreed very well. In polymeric cellulose, also leaving group effects of the *O*-4 and *O*-1 glucopyranosyl anions come into play. Calculations indicated the O-4 anion to be more stable, and hence the better leaving group. In actual cellulose, the degradation starting from 3-keto units will become even more dominant than in the model compound, suggesting that

Electronic supplementary material The online version of this article (https://doi.org/10.1007/s10570-018-1835-y) contains supplementary material, which is available to authorized users.

T. Hosoya
Graduate School of Life and Environmental Sciences, Kyoto Prefectural University, 1-5 Hangi-cho, Shimogamo, Sakyo-ku, Kyoto 606-8522, Japan

M. Bacher · A. Potthast · T. Rosenau (✉)
Division of Chemistry of Renewables, Department of Chemistry, University of Natural Resources and Life Sciences Vienna, Muthgasse 18, 1190 Vienna, Austria
e-mail: thomas.rosenau@boku.ac.at

T. Elder
USDA-Forest Service, Southern Research Station, 521 Devall Dr., Auburn, AL 36849, USA

T. Rosenau
Johan Gadolin Process Chemistry Centre, Åbo Akademi University, Porthansgatan 3, 20500 Turku, Finland

carbonyls at C-2 and C-3, both of which afford the C-2 enolate due to the rapid interconversion between the C-2 and C-3 enolates, are chiefly responsible for alkali-induced chain cleavage in oxidatively damaged cellulose, while an aldehyde at C-6 is more innocent.

Graphical Abstract

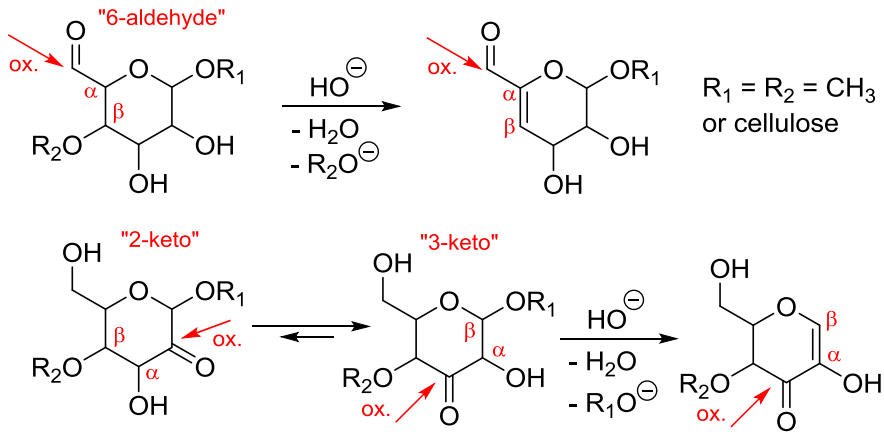

Keywords Cellulose · Cellulose oxidation · Aging · Beta-elimination · Carbonyl groups · Cellulose degradation

Introduction

The pulp and paper industries are an important mainstay of many national economies worldwide. This is somewhat contrasting with the general perception of cellulosics as being conventional, relatively low-cost bulk products. Cellulosic products are widely seen as "being there anyway", as commodities that are produced in huge amounts, having been around already for decades, if not centuries. Cellulosics are usually not perceived as high-tech materials and are rarely linked to cutting-edge research in the mind of the users and customers. Novel products usually do not intrigue customers as fancy cell phones, the newest cars or advanced computer technologies do. Only recent developments, being connected to increased environmental awareness worldwide, recognition of global problems, and the advent of bioeconomies and biorefineries, have brought back cellulosics into public perception as valuable biomaterials. In this context, the pulp and paper industries are increasingly regarded as a business in which high-tech and innovation are very well present. The emergence of biorefinery concepts has also newly stressed the recycling, biomineralization and aging aspects of (ligno)celluloses. Sustainability in a material science sense—aging, degradation, durability, properties changing over time—became hot topics. Many studies dealing with cellulose degradation, damage, yellowing and aging, coming from "classical" pulping and bleaching chemistry or from conservational science in the second half of the twentieth century, have thus been "re-discovered" or repeated, and several new ones have been added.

It is a long and well established fact that cellulose oxidation chiefly influences its properties (Lewin 1997; Potthast et al. 2006). While "cellulose oxidation" is, in principle, well-defined and can be related to precise chemical structures and structural changes (see below), it is only one single aspect of cellulose aging and not synonymous with it. "Cellulose aging" is a rather nebulous term, and the particular aspect of importance lies in the eye of the beholder: natural aging (Whitmore 2011), yellowing of freshly produced pulp upon transportation (Forsskahl 1994; Sevastyanova et al. 2005), brittleness of historic papers (Luner 1988), changed surface properties of cellulosic materials (Kato and Cameron 1999; Sutý et al. 2012), strength losses of cellulosic textiles (Uddin et al. 2015; Block 1982), structural changes upon alkaline treatment of cellulosic fibers (Öztürk et al. 2009; Eronen et al. 2009), cellulose degradation

during ripening of alkali cellulose in rayon production or upon alkali treatment in cellulose ether production (Freytag and Donze 1983; Lewin 1965), molecular weight losses upon cellulose dissolution (Rosenau et al. 2005a, b; Potthast et al. 2002)—all these facets are consequences of cellulose oxidation and can eventually be traced back to the same chemistry.

In many cases, especially when dealing with modern pulps and cellulosic products, cellulose oxidation is caused by pulp processing, mainly during the various bleaching steps. Oxidative bleaching agents that are supposed to attack chromophores and residual lignin might act less selectively than in the ideal case, and might also harm carbohydrate structures, in particular cellulose. In other instances, oxidation can also be a consequence of "conventional" cellulose aging (Zervos 2010), for which the causes and influencing factors are manifold: exposure to environmental stressors, light and irradiation, thermal stress, oxidants (also mere air), pollutants, humidity changes, or simply long-term exposure to ambient atmosphere (Potthast et al. 2004; Henniges et al. 2012; Kolar 1997; Wilsoin and Parks 1979). As diverse as the causes might be, their primary effect is astonishingly simple: cellulosic hydroxyl groups are converted either to carbonyl structures (keto groups at C-2 or C-3, aldehyde groups at C-6) or carboxyl moieties (only possible at C-6 and at the reducing end) (Rosenau et al. 2005a, b). There are no other options in a cellulose molecule with regard to the basic oxidation steps (when the minute contribution of the terminal reducing end and the proximal 4-OH group is neglected). Per se, such an oxidation of hydroxyl groups does not affect the molecular weight distribution as it does not change the celluloses´ chain length. (Of course, there are other cellulose oxidations, such as by periodate or TEMPO, which by subsequent processes change molecular weight and solution properties—but these processes are deliberate modifications and do not fall within the scope of conventional aging).

Molecular weight losses—or in other word cellulose chain cleavage—are a later consequence of the initial oxidation, i.e. a subsequent process, but not a direct outcome of the initial oxidation itself. The process of β-alkoxy-elimination has early been recognized as the actual cleavage mechanism in oxidized celluloses. It starts from any carbonyl (C=O) moiety, no matter whether it is located at C-2, C-3, or C-6, and causes cleavage of the adjacent glycosidic bond in β-position. This means that an alkoxy substituent is lost from the next-but-one carbon, seen from the viewpoint of the sp^2-carbon that carries the carbonyl oxygen. However, only in recent years the generality of the reaction has been recognized as a fundamental, nearly ubiquitous process in cellulose oxidation and aging chemistry (Blazej and Kosik 1985; Potthast et al. 2007; Golova and Nosova 1973). Generally induced by alkali, the reaction starts already at slightly-above-neutral pH values of 8–9. Thus, by any carbonyl along the cellulose chain, a "predetermined breaking point" has been introduced, where chain cleavage will preferably occur. Imagine a cellulose molecule of 1000 anhydroglucose units (AGUs) which experiences very minor oxidation—only four hydroxyl groups out of the 3000 in the 1000 AGUs. Assuming equal spacing of the introduced four carbonyl groups, slightly alkaline conditions will cause immediate fragmentation into five cellulose molecules of merely 200 AGUs—a dramatic effect, but nicely illustrating the drastic outcome that very minor oxidation can have on the molecular weight. The β-elimination reaction was even employed as a diagnostic tool, using the lengths of chain fragments to calculate back, where oxidation must have occurred in the original, long cellulose chains (Potthast et al. 2009). The reaction is also known to be the reason for drastic molecular weight losses upon TEMPO oxidation (Hiraoki et al. 2015; Shibata and Isogai 2003; Isogai and Kato 1998; Zimmermann et al. 2016) or periodate oxidation (Potthast et al. 2007; Sulaeva et al. 2015; Calvini and Gorassini 2012; Kristiansen et al. 2010), and it has been recognized as one key process in processes that cause degradation in old books, manuscripts and valuable historic documents in general.

Apart from its obvious generality and predominance in cellulose (aging) chemistry and the preponderance of its consequence, namely cellulose chain cleavage, the β-alkoxy-elimination itself is still an unknown entity, its detailed stepwise mechanism and possible rate differences according to the oxidation positions being unknown. This was the starting point for the present study—to have a closer look into the molecular mechanism of the β-alkoxy-elimination in celluloses, and to establish whether the oxidation site might have any effect on regioselectivity or rate. The experiments for model compounds and cellulose are correlated with computational results, and the outcome is critically discussed.

Materials and methods

General

Thin layer chromatography (TLC) was performed on Silica gel 60 F254 pre-coated glass plates (Merck). Flash column chromatography was performed on Silica gel 60 from Merck (Darmstadt, Germany). Solvents were purchased in synthesis grade from Roth, Sigma-Aldrich and VWR and were used as received. Reagents were obtained from Sigma-Aldrich, TCI and Fluka. Melting points were determined on a Kofler hot stage microscope and are uncorrected. Elemental analyses were performed on a EURO EA 3000 CHNS-O instrument from HEKAtech (Wegberg, Germany) at the Microanalytical Laboratory of Vienna University.

NMR spectra were recorded on a Bruker Avance II 400 instrument (Rheinstetten, Germany) with a resonance frequency of 400.13 MHz for ^{1}H and 100.62 MHz for ^{13}C. The samples were dissolved in $CDCl_3$ or DMSO-d_6 for characterization or D_2O/NaOD for kinetic studies (99.8%D, Euriso-top, Saint-Aubin, France). Raw data processing was carried out with ACD/NMR Processor Academic Edition. The chemical shift values are given in δ ppm values relative to TMS, respective coupling constants are given in Hz.

FTIR experiments were performed on a Perkin-Elmer Frontier IR Single-Range spectrometer (Waltham, Massachusetts, USA) in ATR mode (diamond/ZnSe crystal, $LiTaO_3$ detector, KBr windows).

Kinetic experiments

Conditions of the kinetic experiments and variations of the reaction parameters (temperature, concentration, pH) are discussed in the main text.

Model compounds **1**–**5**

Methyl 4-*O*-methyl-β-D-glucopyranoside (**1**) and the products representing a "6-keto-AGU" (**2**), "3-keto-AGU" (**3**), "2-keto-AGU" (**4**), and 6-carboxyl-AGU (**5**) (Scheme 1) were available from previous studies (Röhrling et al. 2001; Krainz et al. 2010). Integrity and purity of the compounds were confirmed by NMR and elemental analysis, and all analytical data agreed with those in the literature (Röhrling et al. 2001; Krainz et al. 2010).

Computations

The GAUSSIAN 09 program packages were employed (Frisch et al. 2009). Geometry optimization was carried out according to the M06-2X density functional theory (DFT) method (Zhao and Truhlar 2008). The 6-311+G(d,p) basis sets were employed for H, C, O, where the diffuse function on H was omitted. Frequency calculations verified the identification of an energetic minimum (no imaginary frequencies). Reactant and product of transition states were confirmed by geometry optimization with the steepest descent method instead of intrinsic reaction coordinate (IRC) calculation. We started the geometry optimization of transition states from a pre-optimized geometry with the bond to be broken extended. In the case of C1-OMe to be cleaved, for instance, this bond was elongated to around 2.5 Å, and the optimization was started. The analytical Hessian matrix was calculated in the first step of the optimization. The zero-point energy of optimized species was evaluated by frequency calculation at the DFT(M06-2X) level of theory. We also evaluated the entropy of the optimized species at 298.15 K in the frequency calculation to estimate the Gibbs energy. In this case, the translational entropy of the solute in water was computationally treated according to the literature (Mammen et al. 1998). The potential energy of the optimized geometry was calculated at the MP4(SDQ) level with better basis sets: 6-311+G(2d,2p), where again the diffuse function was not introduced to H. The MP4(SDQ) potential energy was corrected with the above zero-point energy calculated at the DFT(M062X) level. In all calculations, solvation energy in water was evaluated with the polarizable continuum model (PCM) method, where the UFF parameters (the default setting in Gaussian09) were used to determine the cavity size.

Results and discussion

Experimental studies

This study makes use of appropriate cellulose model compounds. This is necessary because the exact

oxidation positions and subsequent structural changes cannot be analytically monitored directly for polymeric cellulose. As precursor model compound—similar to previous studies which established its high suitability to mimic cellulose—methyl 4-*O*-methyl-β-D-glucopyranoside (**1**) has been used (Yoneda et al. 2015; Mackie et al. 2002). The compound represents one AGU along a cellulose chain, with the two methyl groups representing the truncated cellulose chains that would extend to both sides of this AGU in the polymer. The 4-*O*-methyl group is crucial to render the hydrogen bond network in the solid model compound more similar to that of celluloses (cellulose II). Simple methyl β-D-glucopyranoside (without the 4-*O*-methyl group) would thus be inferior as model compound. Synthesis of model compound **1** has been described in our previous work, as has the synthesis of the selectively oxidized derivatives **2**–**4**. Model compound **1** was subsequently oxidized at either C-6, C-3 or C-2, according to literature protocols (Röhrling et al. 2001; Adorjan et al. 2004; Krainz et al. 2010), the products representing a "6-keto-AGU" (**2**), "3-keto-AGU" (**3**) and "2-keto-AGU" (**4**) in an oxidatively damaged cellulose chain, see Scheme 1. While oxidation at C-2 and C-3 evidently generates a ketone (C=O), oxidation at C-6 affords an aldehyde (CHO). In aqueous solution, **3** and **4** are present exclusively as the "proper" ketones with sp^2-carbonyl carbons, while the C6-aldehyde compound **2** is in equilibrium with its sp^3-hybridized aldehyde hydrate ($C(OH)_2$) (Röhrling et al. 2001). Compound **5**, a glucuronic acid derivative, i.e. having a 5-carboxyl group (COOH), was used for reasons of comparison (Bohrn et al. 2005), in order to establish whether a carboxyl moiety might introduce instabilities similar to carbonyl functionalities.

In order to draw conclusions if and how the oxidation position influences the rate of the β-elimination, the two substituents at C-1 and C-4 must be the same (although in cellulose they are evidently not) to exclude that structural effects of the substituents superimpose or overrun possible effects of the oxidation position. For example, phenyl 4-*O*-methyl-β-D-glucopyranoside would have two dissimilar substituents with the phenoxyl anion being a good nucleofuge (stable anion) and the methoxyl group being a less stabilized one: rate differences in the β-elimination in that case would thus not solely be related to oxidation positions, but also to the stabilities of the leaving anions. The necessity of the same 1- and 4-substituent (to exclude leaving group effects) means a drawback at the same time: the eliminated group is always methanol so that information about its origin is lost, at least if only the eliminated methanol and not the residual pyranose product is monitored. We expected this issue to get important in the case of the 2-keto (**4**) and the 3-keto derivative (**3**), which are readily interconverted via the 2,3-enediol. Only from analyzing the eliminated methanol it would not be possible to say whether the 2-keto compound **4** was the actual precursor (eliminating the 4-*O*-methyl substituent) or the 3-keto compound **3** (eliminating the 1-*O*-methyl group). In the case of the 6-aldehyde compound (**2**), this is evidently no issue because the eliminated methanol can only originate from the 4-*O*-methyl moiety.

To solve this problem—to have the same substituents in 1-position and 4-position while still being able to distinguish them analytically, preferably by NMR spectroscopy—we used a ^{13}C-labeled 4-*O*-methyl moiety, see compounds **1***–**5*** in Scheme 1. By ^{1}H NMR spectroscopy, CH_3OH in natural isotopic abundance (1.1% ^{13}C) and labeled $^{13}CH_3OH$ (> 99% ^{13}C) can be easily distinguished, and their ratio in isotopomeric mixtures quantified. While the methyl´s resonance in CH_3OH is a singlet (3.34 ppm), it becomes a doublet in $^{13}CH_3OH$ due to the heteronuclear coupling with ^{13}C (nuclear spin of ½). In addition, the center of this doublet is slightly shifted relative to the CH_3OH-singlet due to a minor isotopic effect of the ^{13}C. The potential isotopic labeling alternative, to use deuteration (CD_3-OH) instead of ^{13}C labeling, is not constructive: it would imply ^{13}C NMR detection which is too slow to follow reaction kinetics in the present case. Moreover, reliable integration of the ^{13}C resonances (C bound to H or D) would require pulse sequences that additionally increase measurement time relative to a standard ^{13}C experiment.

We followed the alkaline-induced degradation of the model compounds (see Scheme 2) by means of ^{1}H NMR, recording the increasing signal of liberated methanol. Kinetics was recorded with the same setup, using solvents of preset temperature into which the model compounds were added, subsequently recording the spectra at the same temperature. The temperature range of that kinetics was set between 10 and 70 °C in 10 °C-intervals. Just from simple visual observation, degradation of all three model

Scheme 1 Model compounds **1**–**5** and isotopically labeled (^{13}C) model compounds **1***–**5*** used in this study

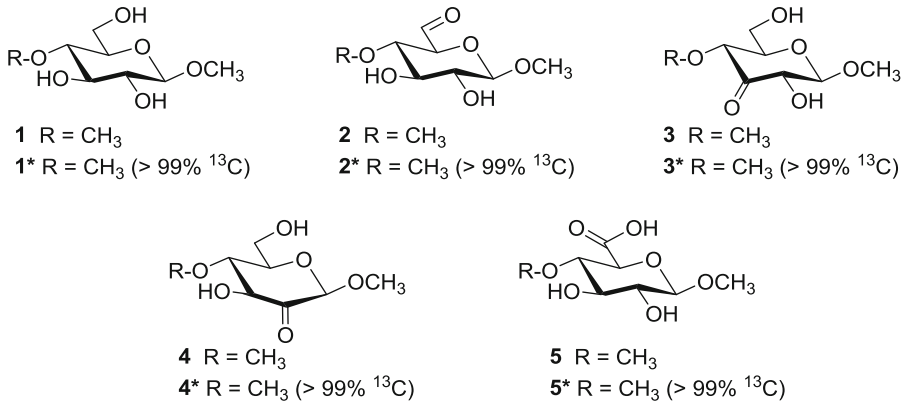

compounds was easily discernible as it was accompanied by a slightly yellow discoloration.

In a first set of experiments, we followed the degradation of the model compounds at different pH values and ambient temperature. Going from pH = 6 to pH = 13 in 0.5 intervals, the reaction rate was initially very low, showed a sharp increase between pH 8 and 8.5, and remained constant at pH values above 9.5, for all three compounds. The HO^- concentration thus did not seem to affect the rate law uniformly, and HO^- was evidently not a part of the rate-determining elemental step in the reaction sequence. It seemed logical to assume that HO^-, acting as a base, exerted a deprotonating action, which around the pK_A of the acidic position became dominant. Note that at the half-neutralization point pH value and pK_A value get equal. At higher pH values, deprotonation would be complete so that no further rate effects were seen. A linear dependence between the concentration of the model compound and the reaction rate was observed. The kinetics of the β-elimination reaction was thus following a first-order rate law, expressed by:

$$r = \mathrm{d[A]/dt} = k[\mathrm{A}] \quad (1)$$

with [A] being the concentration of the model compound, k the kinetic rate constant, and r the reaction rate. Both r and k are temperature-dependent. At pH values above 9, i.e. [HO^-] above 10^{-5} M, the hydroxyl concentration is large relative to that of the model compound, i.e. [HO^-]≫[A] and can be considered constant, the deprotonation equilibrium being fully on the side of the anion, and equilibration being immediate.

When the kinetics of model compound consumption was followed at 20 °C and pH = 11, the ln[A] versus t curve was a straight line for all three model compounds, confirming the first reaction order (Fig. 1). The kinetic rate constants for the C6-aldehyde-compound **2**, the 2-keto-compound **4** and the 3-keto-counterpart **3** had a ratio of 1:5:22, indicating the 3-keto compound to be the least stable one (see Scheme 2). In a mixture of the three compounds, **3** had been already completely degraded when only about 5% of **2** was consumed. Glucuronic acid model compound **5** was completely stable under the conditions used and showed no chemical changes whatsoever. The numerical values for the kinetic rate constants retrieved from the slope of the regression lines in Fig. 1 are summarized in Table 1. The half-times of the degradation $\tau_{1/2}$, i.e. the times at which concentration of the educt decreased to half of the starting concentration, allow an easy comparison of the compounds´ reaction rates (cf. Table 1). Note that $\tau_{1/2}$ of first-order reactions is independent of the starting concentration:

$$\tau_{1/2} = \ln 2/k \quad (2)$$

with k being defined according to Eq. 1 above.

These results offer two interesting general conclusions: first, keto functionalities at C-2 or C-3 are apparently much more relevant with regard to cellulose instability and β-elimination than the C6-aldehyde. Second, the "harmfulness" of C6-oxidation to the aldehyde stage can be completely eliminated by further oxidation to the carboxylic acid (*cf.* compound **5**), which—with regard to proneness toward β-elimination—is equally innocent as the starting material with its C6-hydroxymethyl group.

By recording the degradation kinetics (NMR) in 10 °C steps from 10 °C up to 70 °C, the temperature dependence of the β-elimination rates for compounds **2–4** was determined (compound **5** was left out as it was stable, see above). Since the possibility existed that reaction intermediates might react with the methanol already formed, we used only initial reaction rates (up to 20% conversion) to rule out that kinetics were significantly influenced by side reactions. However, the almost perfect linearity over the whole concentration range indicated that such side reactions were absent anyway. From the temperature data, the Arrhenius activation energy E_a was retrieved based on the logarithmic representation of the Arrhenius equation (Eq. 3), E_a being (− 1/R) times the slope of a regression plot of ln(k) versus (1/T).

$$k = Ae^{-E_a/RT} \tag{3}$$

The activation parameters of Arrhenius equation (Eq. 3) and Eyring equation (Eq. 4) are linked through Eq. 5. The linearized Eyring equation (Eq. 6) was used to obtain the activation parameters $\Delta H^{\ddagger}$, $\Delta S^{\ddagger}$, and $\Delta G^{\ddagger} = \Delta H^{\ddagger} - T\Delta S^{\ddagger}$ from the kinetic data in a plot of ln (k/T) versus 1/T. The E_a and $\Delta H^{\ddagger}$ values evidently reflected the reactivity orders in the same way as the kinetic rate constants did: the largest kinetic rate constant corresponds to the lowest activation energy.

$$k = \frac{k_B T}{h} \times e^{\Delta S^{\neq}/R} \times e^{-\Delta H^{\neq}/RT} \tag{4}$$

$$E_a = \Delta H^{\ddagger} + \mathrm{RT} \tag{5}$$

$$ln\frac{k}{T} = \frac{-\Delta H^{\neq}}{RT} + ln\frac{k_B}{h} + \frac{\Delta S^{\neq}}{R} \tag{6}$$

The activation parameters for the degradation of the three model compounds **2–4** are summarized in Table 2.

The activation entropies $\Delta S^{\ddagger}$ were positive for all three model compounds, indicating that the transition state of the rate-determining step is of lower order than the isolated reactants. This is logical for the reaction since the transition state exhibits extended lengths of the bonds which are broken later on the reaction coordinate of the elemental step. Connected to this, there is a considerable entropy loss with concomitant gain of vibrational, translational, and rotational degrees of freedom. Interestingly, the activation

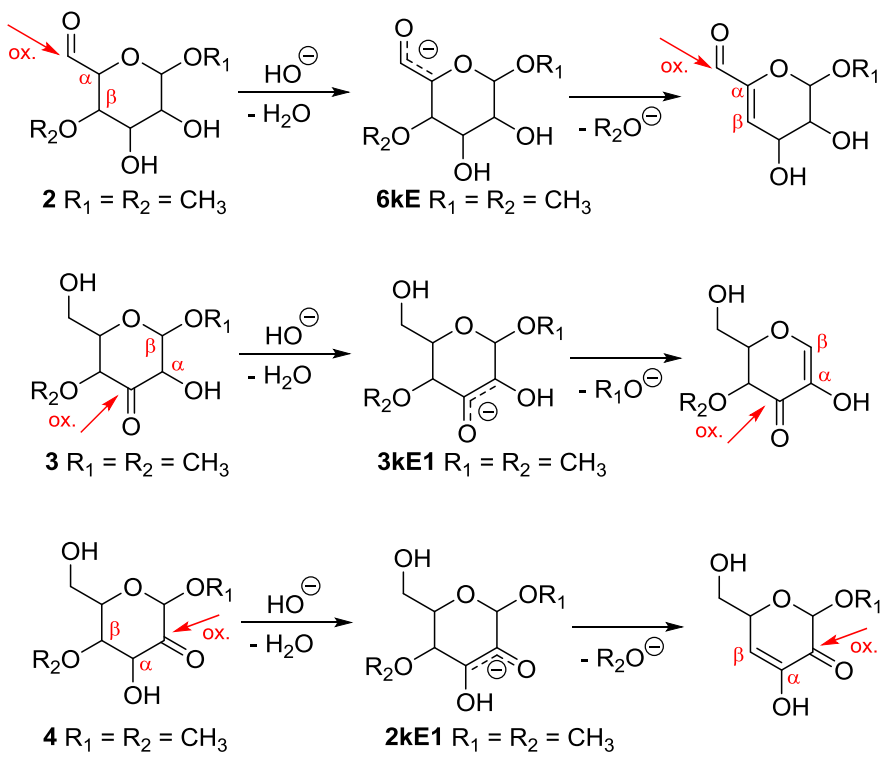

Scheme 2 Alkali-triggered β-elimination reaction starting from oxidized anhydroglucose units, ox., α and β (in red) indicating the oxidized position and the neighboring α- and β-carbons, respectively. Model compounds: R = CH_3, cellulose: R = cellulose chain. **6kE**, **2kE1** and **3kE1** denote the intermediate enolate forms. The stereochemistry has not been displayed for reasons of clarity and easy comparability

entropy was somewhat more positive—by about 6.5 cal/(mol K)—for the 6-keto compound **2** than for the 2-keto and 3-keto compounds **4** and **3**. Apparently, the degree of order is more strongly lowered when the exocyclic C-6 is involved in enolate formation than in the cases of the ring-centered enolates.

An additional piece of experimental evidence was provided by analysis of the cleaved-off methanol for the isotopomeric compounds **2***–**4***, carrying a 4-*O*-$^{13}CH_3$ group while the glycosidic methyl group had normal isotopic abundance. Aldehyde **2*** was the "easy case": the eliminated group was evidently only ^{13}C-methanol, with no ^{12}C-compound being present. Thus, elimination of the 4-*O*-substituent (and only of this one) occurred, which is fully in-line with the mechanism in Scheme 2. The situation for the two keto-compounds **4*** (2-keto) and **3*** (3-keto) is somewhat more complicated: if solely considering the β-elimination mechanism, one would expect elimination of the 4-*O*-substituent as $^{13}CH_3OH$ from the 2-keto-compound **4** and CH_3OH from C1 in the 3-keto-compound **3**. However, these pathways are superimposed by the easy interconversion of the 3-keto enolate **3kE1** and the 2-keto enolate **2kE1** (Fig. 5), which could influence the selectivity of the elimination. As presented in Fig. 2, at pH (pD) values above 10, only the aglycon, the "glycosidic methanol", was eliminated, no matter whether starting from 2-keto-compound **4** or from 3-keto-compound **3**. The 4-*O*-methyl-substituent was never cleaved off, either from the 2-keto- or from the 3-keto-compound: ^{13}C-methanol was only present in natural abundance (seen by the "normal" ^{13}C-satellites). At lower pH (pD) values between 8 and 10, there were small amounts (< 11%) of $^{13}CH_3OH$ found, its concentration decreasing with pH and becoming zero at a pH of 10 and above. The differences between the two starting compounds **3** and **4** were negligible, and were much smaller than the (already tiny) differences caused by different pH values (Fig. 2).

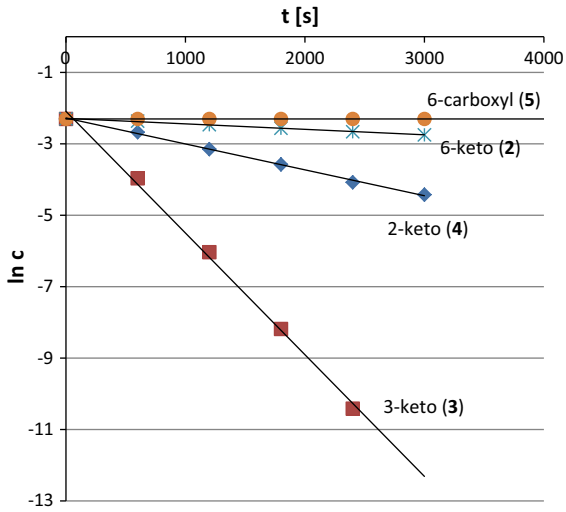

Fig. 1 Degradation of the model compounds **2**–**5** by alkali (NaOD in D_2O, pD = 11) at 20 °C. The linearity of the ln c versus t graphs indicates first-order kinetics. Measurement of compound **3** was stopped at 2400 s (complete consumption)

This allows the important conclusion that under conditions of the alkali-triggered β-elimination compounds **3** and **4** behave similarly. Elimination starts from the common 3-keto enolate intermediate, which is formed directly from 3-keto-compound **3**, but also by enolate interconversion from 2-keto-compound **4**. In other words, an oxidized anhydroglucose unit in cellulose will eliminate, quite selectively, the "1-substituent chain part", no matter whether C-2 or C-3 carried the keto group. In the case of a C6-aldehyde, the "4-substituent chain part" will be cleaved off.

As a side observation, the outcome of thermal, i.e. not alkali-triggered, eliminations, e.g. at 80 °C and pH 7, is quite different, with a $^{13}CH_3OH/CH_3OH$ ratio of 71/29 starting from 3-keto-compound **3** and a ratio of 46/54 from 2-keto-compound **4**. This points to a different mechanism with the enolate forms being less decisive. The thermal elimination reactions were not further studied.

Computational studies

The computational part of this study addresses in detail the degradation mechanisms of oxidized

Table 1 Degradation of the model compounds **2**–**5** by alkali (NaOD in D_2O, pD = 11) at 20 °C

Compound	k (s^{-1})	$\tau_{1/2}$ (s)	r rel. to **2**
2 (6-keto)	1.53×10^{-4}	4530.4	1.00
4 (2-keto)	7.82×10^{-4}	886.4	5.11
3 (3-keto)	3.38×10^{-3}	205.1	22.53
5 (6-carboxyl)	0.00	–	–

Rate constants k (s^{-1}), half-times $\tau_{1/2}$ (s) and reaction rates r relative to compound **2** (rounded to the first decimal)

anhydroglucose units in model compounds and cellulose (see Scheme 2) through β-fragmentation of the corresponding enolates that were formed under alkaline conditions. β-Alkoxy-elimination proceeds only in—at least slightly—alkaline media and starts from the corresponding enolate structure (Scheme 2). If other acidic sites in the molecules are present that also can be deprotonated, such as the carboxyl group in model compound **5**, this is irrelevant to the actual β-elimination process. Only abstraction of an α-proton (a proton at the carbon directly adjacent to the carbonyl position) initiates the β-alkoxy-elimination process. The α-proton is rendered acidic through the electronic effect of the neighboring carbonyl group ("methylene activity"), this behavior being very well known from aldol chemistry. The detailed degradation involves three analogous pathways which differ according to the starting position, the position of the proton abstraction for enolate formation, and the eliminated substituent (see Scheme 2). α-C-H proton-abstraction by the base (HO^-) is the first elemental step in all three of them, followed by elimination of the β-substituent.

Although the general mechanisms themselves, as in Scheme 2, are readily predicted from basic organic chemistry principles, an in-depth evaluation is not trivial because there are various factors determining stability of the transition states, such as ring conformation of the enolates, solvent effects, and electronic structures of the ground and transition states. These influential factors can well be different for the three different oxidized sites in AGUs. This study thus addresses the detailed mechanisms of β-elimination from the three possible oxidation sites, focusing on the activation barriers to figure out the most dominant pathway.

C6-aldehyde

The initial proton transfer from C6-aldehyde model compound **2** to HO^- as the base was investigated at the MP4(SDQ)//DFT(M06-2X) level of theory. The proton is removed from C-5, forming an enolate (which is denoted **6kE** enolate in the following). The polarizable continuum model (PCM) solvation method was first employed for the calculation of the energy of this step, which is the difference between the energies of neutral **2** and OH^- versus the corresponding enolate and H_2O. The energy of the enolate was calculated to be 8.1 kcal/mol lower than that of neutral **2**, which is opposing the experimental observation that enolates are less stable than the corresponding neutral aldehydes with OH^- as the base catalysts. Next, a water cluster model with three explicit water molecules and OH^- was used (Fig. 3), in combination with the PCM evaluation of the solvation energy, for detailed geometries (Cartesian coordinates) see the Supporting Information. The Gibbs free energy (ΔG^0) of the resulting 6-keto enolate **6kE** was 7.1 kcal/mol higher than that of the starting neutral model compound **2**, as shown in Fig. 3, which was in agreement with the above-mentioned concept on the lower stability of enolates relative to their parent aldehydes. It is likely that, when the "naked" OH^- molecule is employed in computations, the stabilization of OH^- in water is underestimated, resulting in a seeming destabilization of the reactants. Based on these considerations, we concluded that application of the cluster model is required for a satisfying calculation of the first proton transfer.

In the next reaction step, β-fragmentation of the enolate **6kE** occurs. The computation of this step was carried out without explicit water molecules to reduce computational costs. As the fragmentation itself is a monomolecular elemental step, the transition state

Table 2 Activation parameters for the pseudo-first order degradation of keto-AGU model compounds **2**–**4** by alkaline (NaOD in D_2O, pD = 11) at 20 °C (293.15 K)

Compound	E_a (kcal/mol)	$\Delta H^{\ddagger}$ (kcal/mol)	$\Delta S^{\ddagger}$ [cal/(mol K)]	$\Delta G^{\ddagger}$ (kcal/mol)
2 (6-keto)	32.0	34.4	17.8	29.2
4 (2-keto)	29.6	32.0	11.3	28.7
3 (3-keto)	26.9	29.3	11.0	26.1

E_a, Arrhenius activation energy; $\Delta H^{\ddagger}$, activation enthalpy; $\Delta S^{\ddagger}$, activation entropy at 298.15 K; $\Delta G^{\ddagger}$, free activation energy (Gibbs activation energy) at 293.15 K

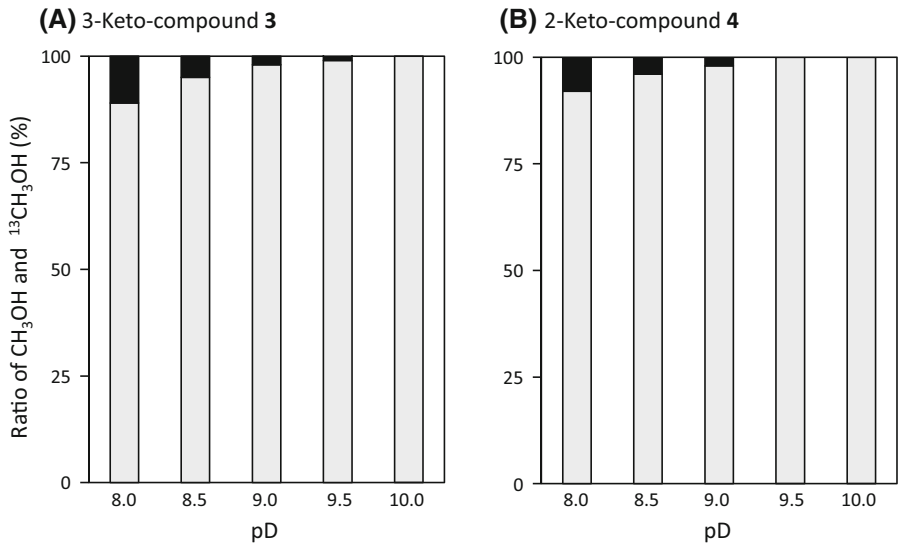

Fig. 2 Ratio between CH_3OH from the 1-*O*-methyl substituent and $^{13}CH_3OH$ from the 4-*O*-methyl substituent after the alkali-triggered β-elimination from the 2-keto- and 3-keto model compounds **3*** and **4***. The formation of $^{13}CH_3OH$ was not observed at pH (pD) values above 10.0

would be dependent on the enolate and its internal geometry, but only little on the medium, so that the error introduced by neglecting explicit water in the computation would be quite minor. The first process involves a conformational change of **6kE** from $^4C_1$ to ^2S_O (Fig. 3), the latter usually being energetically disfavored compared to the former in pyranoses (Ionescu et al. 2005). This conformational change is necessary for π-orbital to overlap with the σ*-orbital of the C4-OMe bond to better accommodate the negative charge in **6kE** in the ^2S_O conformation. As shown in the Newman projections in Fig. 4, this overlap cannot occur in the starting $^4C_1$ conformation. The free activation energy $\Delta G^{0‡}$ of this conformational change was calculated to be relatively small at 12.9 kcal/mol (Fig. 3), and the resulting **6kE**(^2S_O) had the same Gibbs free energy as the **6kE**($^4C_1$). The major reason for the unusually high stability of the ^2S_O conformer relative to $^4C_1$, the π–σ* overlap, can be understood as an analogue of the well-known anomeric effect: the α-anomer of a pyranose being stabilized relative to the β-counterpart by overlapping of one of the O-5 lone pairs and the σ*-orbital of the glycosidic bond (Box 1991). In simple words, the conformational change is preparing the molecule for the fragmentation to occur, by accommodating the sp^2-carbon geometries around the double bond to form and the methoxy group to be eliminated.

The enolate **6kE**(^2S_O) subsequently undergoes C4-OMe cleavage which is not possible (or at least much disfavored) from the $^4C_1$ conformer; it fragments into a product complex **P1** via transition state **TSf1** (Fig. 3). The $\Delta G^{0‡}$ of this process is calculated to be 26.0 kcal/mol relative to the ΔG^0 of **2**($^4C_1$), being clearly more positive than that of the conformational change from $^4C_1$ to ^2S_O. The reaction energy of overall reaction, the energy of **P1** relative to **2**($^4C_1$), was exothermic, $\Delta G^0 = -3.4$ kcal/mol, indicating that the reverse reaction of the β-fragmentation is negligible. It is also noted that the ΔG^0 (– 3.4 kcal/mol) became negative due to the increase in entropy by the β-fragmentation: compare the negative ΔG^0 to the positive potential energy change, $\Delta E = 0.4$ kcal/mol.

C2-keto and C3-keto

By analogy to the 6-aldehyde model in Fig. 3, the energy changes for the proton abstraction from the 2-keto model compound **4** and the 3-keto model compound **3** by OH^- were determined with explicit water and OH^- molecules. The MP4(SDQ)//DFT(M06-2X) calculations indicated that ΔG^0 of **2kE1** relative to **4** and that of **3kE1** relative to **3** were 8.1 and 8.3 kcal/mol, respectively (Fig. 5). These energies are more positive than that in the formation of **6kE** from aldehyde **2** ($\Delta G^0 = 7.1$ kcal/mol, see Fig. 3). This is consistent with general organic chemistry rules that predict enolates from ketones to be less stable than enolates from aldehydes because of the lower acidity (methylene activity) of the α-hydrogen in ketones.

In the case of **3** and **4**, four types of enolates can be formed in principle, **2kE1**, **2kE2**, **3kE1**, and **3kE2**

(Fig. 5). We thus investigated the stability of these enolates with two possible ring conformations: conformations with an equatorial glycosidic bond ($^{O}H_1$/E_1, $^{O}H_5$) and those with an axial glycosidic bond (^5H_O). The MP4(SDQ)//DFT(M06-2X) calculations indicated that the enolate **2kE1** with the ^5H_O ring conformation was the most stable based on Gibbs energy: ΔG^0 of **2kE1**(^5H_O) was 6.3 kcal/mol relative to the reactant **3**($^4C_1$) and this energy is 0.5–8.8 kcal/-mol smaller than that of the other enolates. The enolates **3kE2** and **2kE2** cannot fragment themselves, as the **2kE1** and **3kE1** enolates do. Based on the facts that the enolates **3kE1** and **2kE1** readily interconvert and that the formation of the enolates is a reversible process under ambient condition, all these enolates and the neutral parent carbonyl compounds **3** and **4** are in equilibrium in mild aqueous alkali. Subsequent cleavage according to β-fragmentations means release of methanol (or more correctly methoxyl anions) from C-1 or C-4. The activation energies of these processes will be discussed in the following relative to the most stable compound **3**. The transition states of the conformational changes of the enolates were not calculated, as their activation barriers were expected to be much smaller than those of the subsequent C–O bond cleavage, which seems justified by the above results about the C4–OMe bond cleavage in the degradation of **2** (Fig. 3).

After formation of the enolates, the C1–OMe and the C4–OMe bonds are cleaved through β-fragmentation. In the case of the C1–OMe bond cleavage starting from enolate **3kE1**, the molecule first undergoes a conformational change to ^5H_O, the reason of which being analogous to the one discussed above in Fig. 4: the π-orbital encompassing C-2, C-3, and O-3 can interact with the σ*-orbital of the C1–OMe bond. The $\Delta G^{0‡}$ of this C1–OMe elimination process was calculated to be 24.1 kcal/mol relative to **3** ($^4C_1$), see **TSf2** in Fig. 5. In the case of the C4–OMe bond cleavage, which starts from enolate **2kE1**, both the $^{O}H_5$ and ^5H_O conformers can undergo fragmentation, because both of them have the relevant orbital interactions (Fig. 4). The MP4(SDQ)//DFT(M06-2X) calculations indicated that the pathway starting from the ^5H_O conformer via **TSf3** ($\Delta G^{0‡}$ = 25.7 kcal/mol) was energetically less demanding than the alternative via **TSf4** ($\Delta G^{0‡}$ = 26.8 kcal/mol). The reaction energies of the pathways from **3kE1** and **2kE1** were both negative, $\Delta G^0 = -3.3$ and -8.2 kcal/mol, respectively, indicating that the reverse reactions are negligible as they were in the case of the C-6-aldehyde compound **2**.

Comparison of the three elimination pathways

Among the above quantitatively determined activation barriers of the three pathways, designated as 6-keto-, 2-keto-, and 3-keto-pathways starting from the **6kE**, **2kE1**, and **3kE1** enolates, respectively, the 3-keto-pathway has the lowest Gibbs energy barrier of 24.1 kcal/mol (the others being 25.7 kcal/mol for 2-keto and 26.0 kcal/mol for 6-keto), see Figs. 3 and 5. According to conventional reactivity considerations, however, enolate **6kE** from the aldehyde **2** should be the one which is formed most easily, because of the higher α-acidity of aldehydes. Thus, the higher reactivity of the enolate **3kE1** cannot be explained simply by the stability of the enolates—there must be other factors that favor the 3-keto-pathway, which overcompensate the actually disfavored enolate formation from the ketones **3** and **4**.

Figure 6 presents the geometries of the corresponding transition states **TSf2** and **TSf3**, along with **TSf1** (Fig. 3) for comparison. The C-1–O-5 distance of **TSf2** (1.34 Å) is significantly shorter than that of a normal C-O bond. Also, as shown in Fig. 7, the lowest unoccupied molecular orbital (LUMO) in the pyranose part of **TSf2** shows a p-orbital of C-1 interacting with a p-orbital of O-5 in an anti-bonding way, with the bonding counterpart appearing in the HOMO-13, i.e., thirteen orbitals below the HOMO (highest occupied molecular orbital). These results strongly suggest that one of the lone pairs of O-5 interacts with the C-1 center of the transition state. This double bond character was also indicated by a NBO (natural bond orbital) bond order calculation, affording a value of 1.31 for O-5–C-1. This type of orbital interaction will thus significantly stabilize the transition state, analogous to the O-5–C-1 interaction in oxacarbenium ions (Hosoya et al. 2010). In contrast to **TSf2**, the transition states **TSf1** and **TSf3** do not possess this type of orbital interaction: the C-4–OMe bond in **TSf1** and **TSf3** is a "normal" ether bond without double bond character, resulting in higher activation barriers for the 6-keto- and 2-keto-pathways.

Similar stabilizing effects of the O-5 lone pair have previously been investigated in anhydrosugar formation from phenyl β-D-glucopyranoside under basic

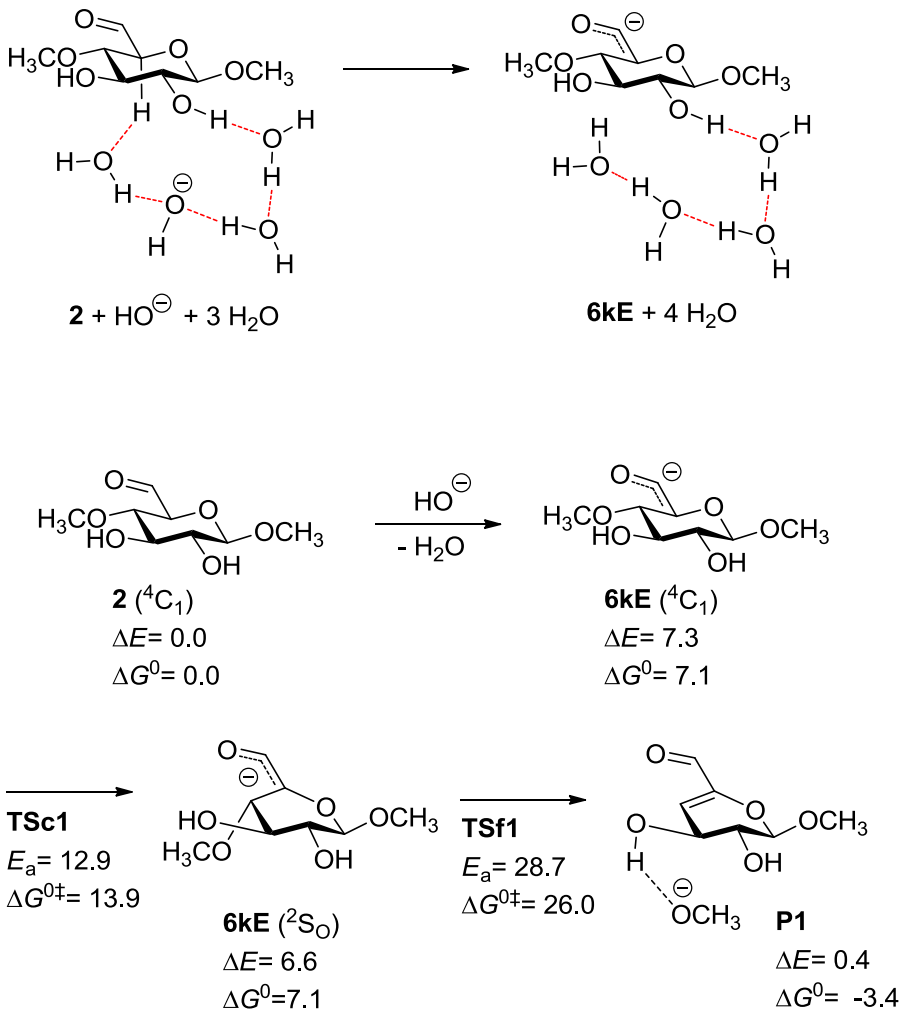

Fig. 3 Upper line: schematic of the proton transfer from **2** to OH^- to form enolate **6kE**, employing a cluster model with three explicit water molecules and HO^-. Middle and lower lines: detailed mechanism of the degradation of the C6-aldehyde model **2** via enolate **6kE**, calculated at the MP4(SDQ)//DFT(M06-2X) level. The energies of the intermediate and the transition states are given in kcal/mol, relative to the reactant **2** ($^4C_1$). See the Supporting Information for how to evaluate the energies of the differently calculated species

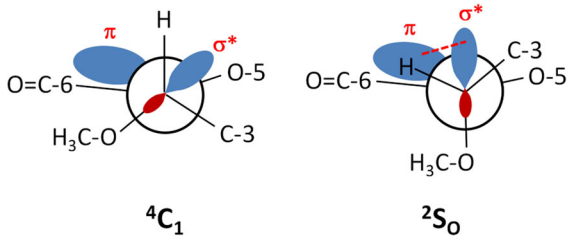

Fig. 4 Newman projections of the $^4C_1$ and ^2S_O conformers of the enolate **6kE** along the C-4–C-5 bond

conditions (Hosoya et al. 2010). That MP4(SDQ)//DFT(B3LYP) level computation suggested that the ring oxygen of the glucoside stabilizes an oxacarbenium ion-like transition state by around 4.0 kcal/mol. On the other hand, the difference in Gibbs energy between **TSf2** and **TSf3** (1.6 kcal/mol) is lower than that value of 4.0 kcal/mol. Likely, this is because C-1–O-1 bond (2.10 Å) in **TSf2** is shorter than the C-4-O-4 (2.16 Å) in **TSf3** because of the stabilization effect by O-5. This shorter C-1–O-1 distance will give **TSf2** additional stabilization, which reduces the difference in the activation barrier. In fact, the difference in Gibbs energy between **TSf2** and **TSf3** increased to 3.2 kcal/mol when the C1–O1 bond is elongated to the length of the C-4–O-4 in **TSf3** (2.16 Å), and this value after the elongation is in accordance with the above reported value of 4.0 kcal/mol, giving a further support for the effects of the ring oxygen discussed above.

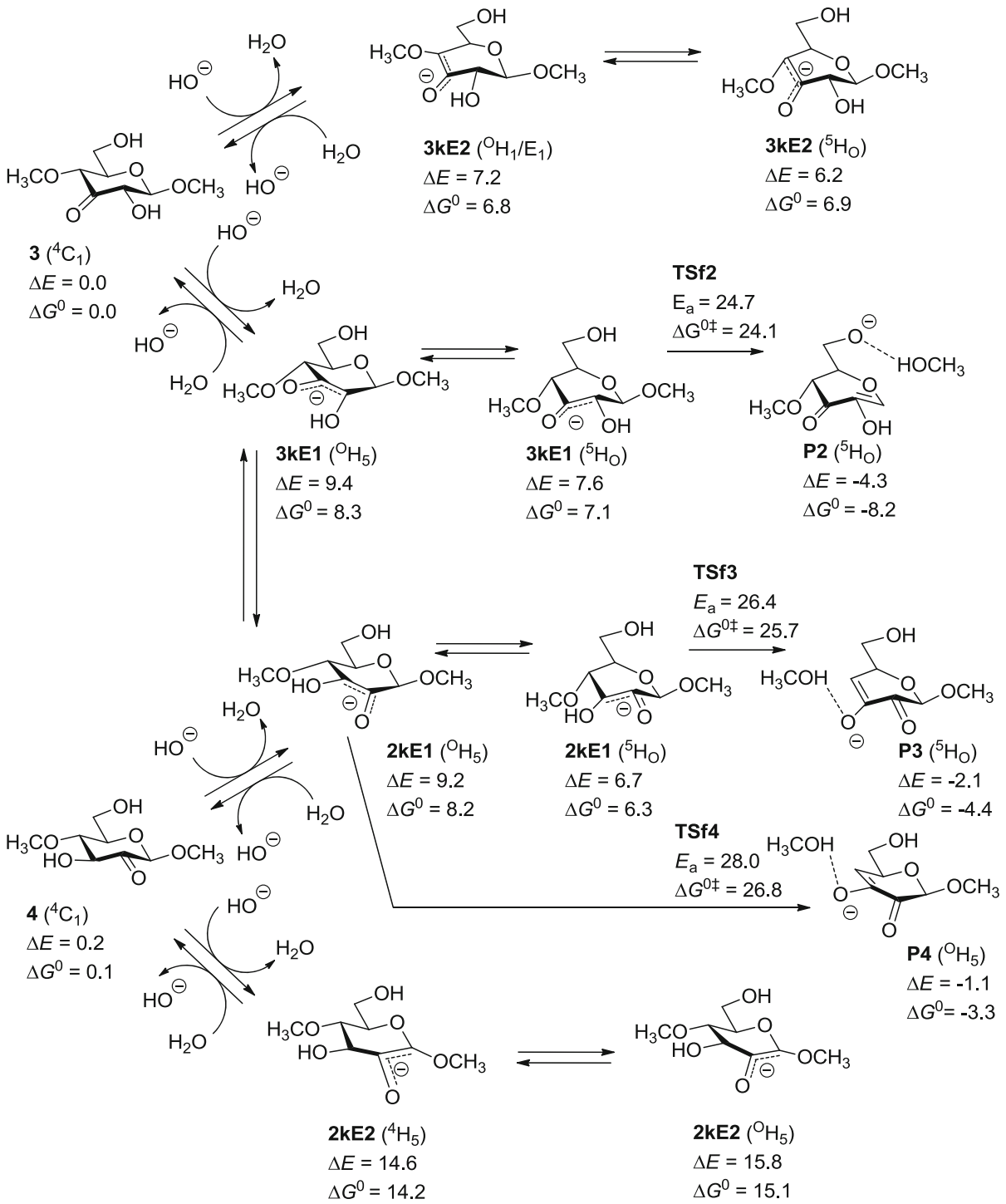

Fig. 5 Detailed mechanism of the degradation of the 2-keto (**4**) and 3-keto (**3**) model compounds via the enolates **2kE1** and **3kE1**, calculated at the MP4(SDQ)//DFT(M06-2X) level of theory. The energies of the intermediate and the transition states are given in kcal/mol, relative to compound **3**($^4C_1$). The energy changes in the first proton transfers, giving the enolates, were calculated with the cluster models similar to that in Fig. 3 (see also Cartesian coordinates in the Supporting Information)

The polymer case—cellulose

The main difference between the three model compounds and actual cellulose—with regard to the β-elimination mechanism—is that in the polymer the two leaving groups at C-1 and C-4 are not the same. Being methoxyl anions formed by either C-1–OMe or C-4–OMe cleavage in the model compounds, the nucleofuge in β-eliminations of cellulose is a glucopyranosyl anion with the negative charge either at O-4 (if eliminated from C-1) or at O-1 (if eliminated from C-4). While 4-OH is a secondary hydroxyl group, 1-OH is a hemiacetal hydroxyl, both being quite different in terms of reactivity, acidity and charge stabilization. This difference in leaving group stability will considerably affect the energetics of each fragmentation pathway. To this end, we evaluated the relative energies of the two β-D-glucopyranosyl anions. As shown in Fig. 8, MP4(SDQ)//DFT(M06-2X) calculations indicated that the O-4 anion was 4.9 kcal/mol more stable than the O-1 anion. As shown in the previous section, the computation of the model system suggested that the 3-keto-pathway is the most dominant. Combining this result with the additional information on the leaving group leads to the idea that the dominance of the 3-keto-pathway becomes even more pronounced in the case of cellulose.

Another expected difference between the model system and actual cellulose is the presence of crystalline structures with strong hydrogen bond networks in cellulose. Oxidized groups may well be present also in crystalline domains, introduced for instance by ionizing radiation. The crystal structure will not only limit the accessibly to alkaline catalysts, but also render the conformational changes necessary for the degradation significantly more unfavorable. DFT(M06-2X) calculations in previous work (Hosoya and Sakaki 2013) have suggested that conformational changes of a anhydroglucose unit in cellulose from $^4C_1$ to $^1C_4$ and $B_{2,5}$ becomes 7–15 kcal/mol more demanding when inter-chain hydrogen bonds are present. Since the ^2S_O and ^5H_O conformations, from which the β-fragmentations start (Figs. 3, 5), are similar to $B_{2,5}$, destabilization of those conformations during β-elimination is also expected. Although non-crystalline, "amorphous" regions of cellulose should be more reactive toward the degradation than crystalline regions because of more disordered inter-chain and intra-chain hydrogen bonds, these considerations strongly suggest that actual cellulose, being an "average" of amorphous and crystalline domains, is much less prone toward alkali-induced β-elimination than the simple monosaccharide model glycosides.

Conclusions

Among the oxidized methyl glucoside model compounds, the 3-keto-pathway from the 3-keto-AGU via the **3kE1** enolate was the most dominant according to our calculations at the MP4(SDQ)//DFT(M06-2X) level of theory, which completely agreed with the experimental facts. This enolate is formed from both the 3-keto compound **3** and the 2-keto compound **4** which are quickly interconverting in alkaline aqueous

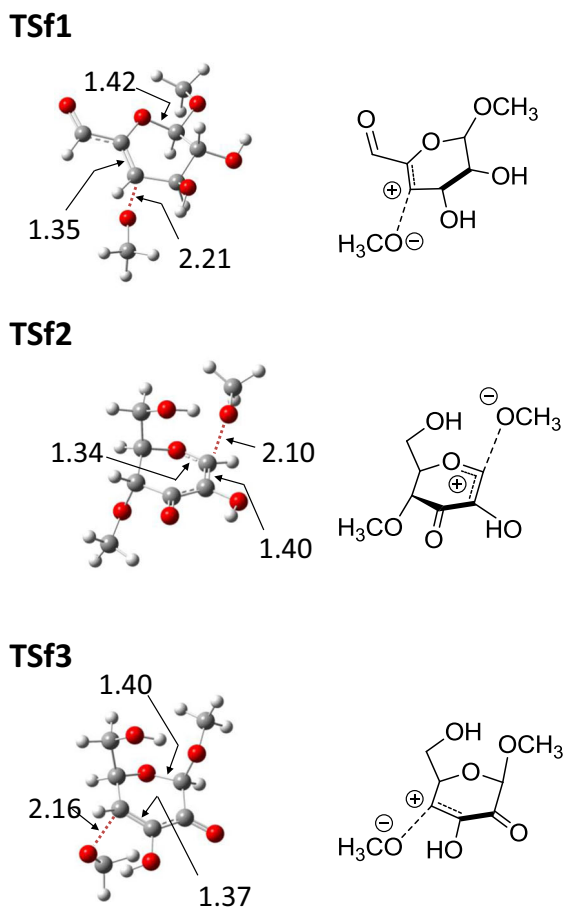

Fig. 6 Transition states **TSf2** and **TSf3** calculated at the DFT(M06-2X) level. Bond lengths are given in Å. **TSf1** (see also Fig. 3) is given for comparison

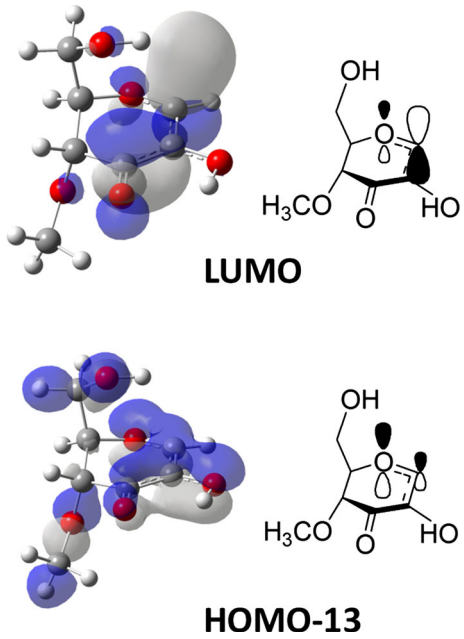

Fig. 7 Molecular orbitals of transition state **TSf2** calculated at the Hartree–Fock level. For a better understanding, the schematic descriptions on the right focus only on the orbital interaction between O-5 and C-1

media at ambient temperature. Structural and orbital analyses of the transition state indicated that the dominance of the 3-keto-pathway was due to stabilization of the transition state leading to the elimination product, by delocalization of the O-5 lone pair to the C-1 anomeric center. Such stabilization does not occur along the 2-keto- and 6-keto-pathways that start from the corresponding 2-keto-AGU and 6-aldehyde-AGU, respectively.

Experimental reaction kinetics of the elimination process provided kinetic rate constants at a relative ratio of 1:5:22 for the degradation of **2**, **3** and **4**, i.e. for the β-alkoxy-elimination triggered by oxidation at C-6, C-2 and C-3, respectively. Chain cleavage following oxidation at C-3 was thus about 22 times faster than cleavage caused by oxidation at C-6, and about four times faster than elimination from the 2-keto-counterpart. In other words, 22 chain cleavages due to C-3 oxidation occur per one cleavage starting from the C-6 aldehyde. The activation energy values, obtained by measurements at different temperatures between 10 and 70 °C, deviated less than 3 kcal/mol from the computed ones (see Figs. 3, 5), experimental and computational results thus agreeing surprisingly well.

In the case of polymeric cellulose, conformational changes of the oxidized AGUs required for the elimination process to proceed are more difficult in crystalline areas with largely intact hydrogen bond system than in amorphous areas. Mechanistically, the stability difference of the leaving groups, the *O*-1- and *O*-4-β-D-glucopyranosyl anions, comes into play and influences the reactivity order of the three pathways in a way that the path via the **3kE1** enolate becomes even more dominant than in the case of the methyl glucoside model system. Chain cleavage caused by C-3- or C-2-oxidation will thus be at least 20 times faster than that caused by C-6 oxidation. Preliminary experiments on mixtures of oxidized cellooligosaccharides indicate average values around 35 (*vs*. 22 for the model compound), i.e. 35 cleavages from C-2/C-3-oxidized cellulose occur per one cleavage from C-6-oxidized cellulose.

These findings are, for instance, interesting with regard to measures to impart increased alkali-stability to celluloses. While mild oxidation with chlorite removes C-6-aldehydes by converting them to carboxylic acids, the effect on the alkaline stability would be only minor, since C-2/C-3 carbonyls, as main causes of alkali instability, remain unchanged. Reductive treatments, affecting all oxidized positions, would be more recommendable in contrast, because also the "faster" C-2/C-3 positions are diminished.

Considering low-degree oxidative cellulose modifications for attachment of reactive anchor groups, periodate oxidation affecting C-2 and C-3 causes higher alkali instability (and in consequence molecular weight loss) than TEMPO oxidation to the

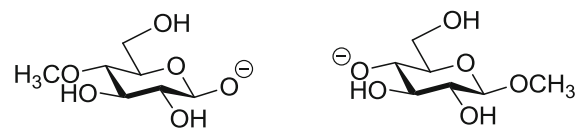

O-1 anion

ΔE = 0.0

ΔG^0 = 0.0

O-4 anion

ΔE = -1.3

ΔG^0 = -4.9

Fig. 8 Relative energies (in kcal/mol) of O-1 and O-4 β-D-glucopyranosyl anions as leaving groups in β-fragmentations of cellulose. Cellulose chains are truncated and replaced by a methyl group for computational treatment

aldehyde stage, at the same molar amount of oxidant, because the TEMPO process is mainly affecting the "less dangerous" C-6.

TEMPO oxidation, because not affecting C-6 fully selectively, will always cause cellulose degradation when carried out in alkaline medium. This is due to the small amount (less than 5% relative to C-6 oxidation) of oxidized C-2-keto and C-3-keto positions which, according to the above results, cause chain fragmentation much faster than from C-6- aldehydes. The contribution of C-6-aldehyde moieties to overall β-elimination is minor, these aldehydes being either intermediates in the oxidation to the carboxyl stage or unwanted leftovers of incomplete oxidation.

With regard to conservation science of cellulosics, different causes of aging will produce different cellulose instabilities. Oxidations as a consequence of transition metal-induced processes, e.g. in iron-gall inks or copper-based paints, generate hydroxyl radicals (besides hydroperoxyl radicals and hydrogen peroxide) which are very reactive and thus show little selectivity, affecting all three positions in cellulose more or less to the same extent. The oxidation at C-2 and C-3 will eventually cause pronounced instability and chain degradation. By contrast, cellulose oxidation by sterically demanding radicals, such as dye radicals or peroxyl radicals, will mainly affect the sterically least demanding and thus better accessible C-6 position. At the same degree of oxidation, the former aged cellulose is much more alkali-labile and more prone to degradation than the latter one.

Apart from these examples, we hope that the mechanistic insights into alkali-induced β-alkoxy elimination in celluloses will also be of interest in other fields of cellulose science and cellulose applications. Since this reaction, being a consequence of oxidative cellulose damage in general, is one of the key processes in cellulose aging and cellulose degradation—with all its different facets in cellulose chemistry and cellulosic material science—its in-depth mechanistic understanding might even prove helpful in areas about which we would not think at present.

Acknowledgments Open access funding provided by University of Natural Resources and Life Sciences Vienna (BOKU). The financial support of the Austrian Research Promotion Agency (FFG, projects "Chromophore I" and "Chromophore II" is gratefully acknowledged. We would like to thank Professor Paul Kosma, BOKU University, Division of Organic Chemistry, for valuable discussions.

References

Adorjan I, Mereiter K, Pauli J, Jäger C, Rosenau T, Potthast A, Kosma P (2004) Crystal and Molecular structure of methyl 4-*O*-methyl-β-D-ribo-hex-3-ulopyranoside. Carbohydr Res 339:795–799. https://doi.org/10.1016/j.carres.2004.01.006

Blazej A, Kosik M (1985) Degradation reactions of cellulose and lignocellulose. In: Kennedy JF (ed) Cellulose and its derivatives: chemistry, biochemistry and applications. Halsted Press, New York, pp 97–117

Block I (1982) The effect of an alkaline rinse on the aging of cellulosic textiles, parts land ii. J Am Inst Conserv 22:25–36. https://doi.org/10.1179/019713682806028504

Bohrn R, Potthast A, Rosenau T, Sixta H, Kosma P (2005) Synthesis and testing of a novel fluorescence label for carboxyls in carbohydrates and cellulosics. Synlett 20:3087–3090. https://doi.org/10.1055/s-2005-921923

Box VGS (1991) The role of lone pair interactions in the chemistry of the monosaccharides. Stereo-electronic effects in unsaturated monosaccharides. Heterocycles 32:795–807. https://doi.org/10.3987/REV-91-425

Calvini P, Gorassini A (2012) Surface and bulk reactions of cellulose oxidation by periodate. A simple kinetic model. Cellulose 19:1107–1114. https://doi.org/10.1021/bm0000337

Eronen P, Österberg M, Jääskeläinen AS (2009) Effect of alkaline treatment on cellulose supramolecular structure studied with combined confocal Raman spectroscopy and atomic force microscopy. Cellulose 16(2):167–178

Forsskahl I (1994) Chromophore changes during bleaching, ageing and irradiation of TCF bleached chemical pulps. Nord Pulp Paper Res J 3:196–202

Freytag R, Donze JJ (1983) Alkali treatment of cellulose fibres. In: Lewin M, Sello SB (eds) Handbook of fiber science and technology, vol. A, part 1. Marcel Dekker, New York, pp 93–165

Frisch MJ et al (2009) Gaussian 09, Revision D.01. Gaussian, Inc., Wallingford

Golova OP, Nosova NI (1973) Degradation of cellulose by alkaline oxidation. Russ Chem Rev 42:327–338

Henniges U, Okubayashi S, Rosenau T, Potthast A (2012) Irradiation of cellulosic pulps: understanding its impact on cellulose oxidation. Biomacromol 13:4171–4178. https://doi.org/10.1021/bm3014457

Hiraoki R, Ono Y, Saito T, Isogai A (2015) Molecular mass and molecular-mass distribution of TEMPO-oxidized celluloses and TEMPO-oxidized cellulose nanofibrils.

Biomacromol 16:675–681. https://doi.org/10.1021/bm501857c

Hosoya T, Sakaki S (2013) Levoglucosan formation from crystalline cellulose: importance of a hydrogen bonding network in the reaction. Chemsuschem 6:2356–2368. https://doi.org/10.1002/cssc.201300338

Hosoya T, Nakao Y, Sato H, Sakaki S (2010) Theoretical study of 1,6-anhydrosugar formation from phenyl D-glucosides under basic condition: reasons for higher reactivity of β-anomer. J Org Chem 75:8400–8409. https://doi.org/10.1021/jo101494g

Ionescu AR, Bérces A, Zgierski MZ, Whitfield DM, Nukada T (2005) Conformational pathways of saturated six-membered rings. A static and dynamical density functional study. J Phys Chem A 109:8096–8105. https://doi.org/10.1021/jp052197t

Isogai A, Kato Y (1998) Preparation of polyuronic acid from cellulose by TEMPO-mediated oxidation. Cellulose 5:153–164. https://doi.org/10.1023/A:1009208603673

Kato KL, Cameron RE (1999) A review of the relationship between thermally-accelerated ageing of paper and hornification. Cellulose 6:23–40

Kolar J (1997) Mechanism of autoxidative degradation of cellulose. Restaurator 18:163–176. https://doi.org/10.1515/rest.1997.18.4.163

Krainz K, Hofinger A, Dietz T, Suess HU, Potthast A, Rosenau T (2010) Synthesis of methyl 4-*O*-methyl-β-D-ribo-hex-3-ulopyranoside-1-^{13}C and methyl 4-*O*-methyl-β-D-ribo-hex- 3-ulopyranoside-3-^{13}C as fragment analogues of oxidized cellulose units. Lett Org Chem 7:186–190. https://doi.org/10.2174/157017810791112478

Kristiansen KA, Potthast A, Christensen BE (2010) Periodate oxidation of polysaccharides for modification of chemical and physical properties. Carbohydr Res 345:1264–1271. https://doi.org/10.1016/j.carres.2010.02.011

Lewin M (1965) The yellowing of cotton cellulose: part III—on the mechanism of yellowing upon aging and alkaline extraction. Text Res J 35:979–986. https://doi.org/10.1177/004051756503501103

Lewin M (1997) Oxidation and aging of cellulose. Macromol Symp 118:715–724. https://doi.org/10.1002/masy.19971180192

Luner P (1988) Evaluation of paper permanence. Wood Sci Technol 22:81–97

Mackie ID, Röhrling J, Gould RO, Walkinshaw M, Potthast A, Rosenau T, Kosma P (2002) Crystal and molecular structure of methyl 4-*O*-methyl-β-D-glucopyranosyl-(1 → 4)-β-D-glucopyranoside. Carbohydr Res 337:161–166. https://doi.org/10.1016/S0008-6215(01)00299-3

Mammen M, Shakhnovich EI, Deutch JM, Whitesides GM (1998) Estimating the entropic cost of self-assembly of multiparticle hydrogen-bonded aggregates based on the cyanuric acid melamine lattice. J Org Chem 63:3821–3830. https://doi.org/10.1021/jo970944f

Öztürk HB, Potthast A, Rosenau T, Abu-Rous M, MacNaughtan B, Schuster KC, Mitchell J, Bechtold T (2009) Changes in the intra- and interfibrillar structure of lyocell (TENCEL®) fibers caused by NaOH treatment. Cellulose 16:37–52. https://doi.org/10.1007/s10570-008-9249-x

Potthast A, Rosenau T, Sartori J, Sixta H, Kosma P (2002) Hydrolytic processes and condensation reactions in the cellulose solvent system N, N-dimethylacetamide/lithium chloride. Part 2: degradation of cellulose. Polymer 44:7–17. https://doi.org/10.1016/S0032-3861(02)00751-6

Potthast A, Schiehser S, Rosenau T, Sixta H, Kosma P (2004) Effect of UV radiation on the carbonyl distribution in different pulps. Holzforschung 58:597–602. https://doi.org/10.1515/hf.2004.113

Potthast A, Rosenau T, Kosma P (2006) Analysis of oxidized functionalities in cellulose. In: Klemm D (ed) Polysaccharides II. Advances in polymer science, vol 205. Springer, Berlin, pp 1–48. https://doi.org/10.1007/12_099

Potthast A, Kostic M, Schiehser S, Kosma P, Rosenau T (2007) Studies on oxidative modifications of cellulose in the periodate system: molecular weight distribution and carbonyl group profiles. Holzforschung 61:662–667. https://doi.org/10.1515/HF.2007.099

Potthast A, Schiehser S, Rosenau T, Kostic M (2009) Oxidative modifications of cellulose in the periodate system—reduction and beta-elimination reactions. Holzforschung 63:12–17. https://doi.org/10.1515/HF.2009.108

Röhrling J, Potthast A, Rosenau T, Lange T, Borgards A, Sixta H, Kosma P (2001) Synthesis and testing of a novel fluorescence label for carbonyls in carbohydrates and cellulosics. Synlett 5:682–684. https://doi.org/10.1055/s-2001-13363

Rosenau T, Potthast A, Milacher W, Adorjan I, Hofinger A, Kosma P (2005a) Discoloration of cellulose solutions in N-methyl-morpholine-N-oxide (Lyocell). Part 2: isolation and identification of chromophores. Cellulose 12:197–208. https://doi.org/10.1007/s10570-004-0210-3

Rosenau T, Potthast A, Kosma P, Saariaho AM, Vuorinen T, Sixta H (2005b) On the nature of carbonyl groups in cellulosic pulps. Cellulose 12(1):43–50

Sevastyanova O, Li J, Gellerstedt G (2005) On the reaction mechanism of thermal yellowing of chemical pulp. Appita Annu Conf 2:517–523. https://doi.org/10.3183/NPPRJ-2006-21-02-p188-192

Shibata I, Isogai A (2003) Depolymerization of cellouronic acid during TEMPO-mediated oxidation. Cellulose 10:151–158. https://doi.org/10.1023/A:1024051514026

Sulaeva I, Klinger KM, Amer H, Henniges U, Rosenau T, Potthast A (2015) Determination of molar mass distributions of highly oxidized dialdehyde cellulose by size exclusion chromatography and asymmetric flow field-flow fractionation. Cellulose 22:3569–3581. https://doi.org/10.1007/s10570-015-0769-x

Sutý Š, Petriláková K, Katuščák S, Kirschnerová S, Jablonský M, Vizarová K, Vrška M (2012) Change in the capability of cellulose fibres to retain water during thermally accelerated ageing of paper. Cellul Chem Technol 46(9–10):631–635

Uddin MG, Islam MM, Islam MR (2015) Effects of reductive stripping of reactive dyes on the quality of cotton fabric. Fash Text 2:8. https://doi.org/10.1186/s40691-015-0032-y

Whitmore PM (2011) Paper ageing and the influence of water. In: Banik G, Brückle I (eds) Paper and water, 1st edn. Elsevier, Amsterdam

Wilsoin WK, Parks EJ (1979) An analysis of the aging of paper: possible reactions and their effects on measurable properties. Restaurator 3:37–62. https://doi.org/10.1515/rest.1979.3.1-2.37

Yoneda Y, Kawai T, Kawada T, Rosenau T (2015) Structural study of methyl glucosides mimicking methyl cellulose. In: Conference Proceedings, 18th ISWFPC International Symposium on Wood, Fibre and Pulping Chemistry, Vienna, Austria, Sept 09–11, vol I. ISBN: 978-3-900932-24-4

Zervos S (2010) Natural and accelerated ageing of cellulose and paper: a literature review. In: Lejeune A, Deprez T (eds) Cellulose: structure and properties, derivatives and industrial uses. Nova Science Publishers, New York, pp 155–203

Zhao Y, Truhlar DG (2008) The M06 suite of density functionals for main group thermochemistry, thermochemical kinetics, noncovalent interactions, excited states, and transition elements: two new functionals and systematic testing of four M06-class functionals and 12 other functionals. Theor Chem Acc 120:215–241. https://doi.org/10.1007/s00214-007-0310-x

Zimmermann R, Müller Y, Freudenberg U, Jehnichen D, Potthast A, Rosenau T, Werner C (2016) Oxidation and structural changes in NMMO-regenerated cellulose films. Cellulose 23:3535–3541. https://doi.org/10.1007/s10570-016-1084-x